

Swelling of colloidal systems

Efrosini Kokkoli and Frank van Swol^{a)}

Department of Chemical Engineering, University of Illinois at Urbana-Champaign, Urbana, Illinois 61801

(Received 1 April 1996; accepted 8 October 1997)

The role of solvent–particle and particle–particle interactions on the swelling of colloidal systems has been investigated. A density functional theory (DFT) approach is taken here to describe a colloid–solvent mixture and develop phase diagrams that give a qualitative picture of possible transitions as a function of the bulk conditions (density and temperature) and the degree of surface solvophobicity. The solvophobicity of the surface is taken as a measure of how much the surface dislikes the solvent, and is determined from the contact angle of the solvent on the surface. The results demonstrate that the nature of the surface (solvophobic or solvophilic) is a key factor in shaping the phase diagrams. For example, when the surface is solvophilic, the dominant phase is the crystalline, where surfaces are spaced by one solvent layer, while when the surface is solvophobic, the system is most often found in the collapsed state (the surfaces are in contact). The shape of the phase diagrams also depends on the particle–particle interaction. When only the repulsive part of the wall–wall interaction is considered, the collapsed phase is observed less frequently and the diagrams are insensitive to the strength of the purely repulsive interaction. In contrast, the strength of the attractive surface–surface potential plays a crucial role in shaping the phase diagrams.

© 1998 American Institute of Physics. [S0021-9606(98)51003-3]

I. INTRODUCTION

Since the 1950's, the central paradigm of colloid science held that electrostatic and electrodynamic (van der Waals) forces were the principal determinants of the state of aggregation of colloid systems. The van der Waals forces are long range, attractive, and arise from the permanent and/or induced dipole–dipole interactions. The electrostatic repulsions arise from like charges on the particle surfaces and overlapping of double layers. These two forces form the basis of the DLVO theory of colloidal stability.^{1,2} Recently, however, experimental and theoretical studies have shown that when two surfaces or particles approach each other closer than a few nanometers, continuum theories of attractive van der Waals and repulsive double-layer forces often fail to describe their interaction. Forces that have been directly measured between minerals and glass,³ all classes of lipid membranes,⁴ biological macromolecules such as DNA double helices,⁵ and proteins⁶ and stiff polysaccharides,⁷ all exhibit features that can not be explained with DLVO theory.

The reversibility, sharpness, reproducibility, and the phase change of clays from a so-called crystalline to swollen gel, show that this transformation is a true thermodynamic transition.⁸ In DLVO theory though, clays are thermodynamically unstable and therefore a reversible change is not possible within its framework.⁹ The sensitivity of clay swelling to temperature and electrolyte concentration also cannot be predicted by this theory, which does not anticipate the high repulsive pressures observed at small separations in clay dispersions (osmotic swelling regime). These short-range forces are dependent on the nature of cations.¹⁰ The

surface force and swelling pressure measurements confirm the existence of a short-range non-DLVO repulsive force. The excess repulsive pressures at small separations have been attributed to changes in the water structure next to the clay layers, similar to the concentration dependent hydration forces observed between mica surfaces.^{11,12} At high electrolyte concentrations, interaction forces between mica sheets can no longer be explained by DLVO theory. A strong repulsive force is observed which does not decay with the expected Debye length and which is of sufficient strength to prevent van der Waals forces from pulling the surfaces into primary minimum contact.¹¹

Biological membranes and macromolecules repel each other and can swell spontaneously. Abrupt changes in surface separation, and the temperature sensitivity of swelling, cannot be predicted by DLVO calculations.^{13,14} The dehydration of silicotungstic acid and lithium silicotungstate occur in a stepwise manner. The crystallization takes place at specific numbers of hydration waters, which are not removed one by one but in specific quantities.^{15,16} This stepwise dehydration behavior is one more case that cannot be explained by the traditional theory.

The failure to describe the phenomena mentioned above is either attributable to the breakdown at small separations of one or both of the continuum theories that form the basis of DLVO theory, or points at the existence of non-DLVO forces. If the DLVO predictions are subtracted from the measured forces, the remaining forces can decay monotonically or be oscillatory with a periodicity equal to the size of the liquid molecules^{17–19} and they can be much stronger than electrostatic or van der Waals interactions. They arise due to a change in the liquid density at the surfaces as they approach each other^{20,21} and are now usually referred to as *solvation forces*. They depend not only on the properties of

^{a)}Present address: Chemical and Nuclear Engineering Department, University of Albuquerque, Albuquerque, New Mexico 87106.

the intervening medium but also on the chemical and physical properties of the surfaces.³

In this paper we present the contribution of oscillatory solvation forces to phase transitions, observed in swelling colloidal systems. Here we choose to consider a simplified model that consists of two smooth parallel plates of area A , separated by a distance h , in a reservoir of solvent. One of the plates is fixed while the other is free to move. The thermodynamic state of the surrounding bulk fluid is fully specified by the system temperature, T , and chemical potential, μ . The key feature of this model, which has made it useful in previous studies,^{22–24} is that it couples a fluid system confined between the surfaces with bulk fluid, at separations where the solvation forces are dominant. The solvation force arises from the structuring of the solvent in the confined space between the plates and is defined per unit area as

$$f_s = \bar{p} - p_b(T, \mu) = - \left(\frac{\partial(\Omega^s/A)}{\partial h} \right)_{T, \mu}, \quad (1)$$

where \bar{p} is the normal component of the force on the moveable wall due to the confined fluid, p_b is the bulk pressure, and Ω^s is the surface free energy of the system. In this case, where we do not consider any additional external pressure (see Ref. 17), the solvation force at equilibrium has to be zero and the equilibrium state of the system, h_{eq} , is found by minimizing Ω^s/A with respect to h . The calculation of the surface free energy is done with the smoothed density functional theory (DFT).²⁵ Molecular dynamics simulations have shown that solvent structuring in confined spaces leads to spatial oscillations in the solvation potential $\Omega^s(h; \mu, T)$, and these oscillations provide the basis for transitions between phases characterized by different h_{eq} .²⁶ The degree of solvophobicity may lead to variations in equilibrium separation between the plates and thus to phase diagrams which vary with the strength of solvent/surface interactions.

The solvophobicity of the surface is taken as a measure of how much the surface dislikes the solvent, and can be determined from the contact angle of the solvent on the surface. Therefore, different solvent/colloid systems with the same degree of wetting (i.e., contact angle), should be represented by the same phase diagram. Most of what we know about the wetting properties of “solid” organic surfaces has been obtained through the application of a very simple experimental procedure, the measurement of contact angles, which is a macroscopic property of the system.²⁷ Contact angles are sensitive to surface structure^{28,29} and provide a useful measurement of the surface wettability.³⁰ In keeping with the approach taken here, Rabinovich and Yoon³¹ also use contact angle to link surface/solvent interactions with solvation forces.

II. DFT AND CONTACT ANGLE

As discussed in the previous section, the determination of phase transitions in interparticle spacing involves the calculation of the free energy of the system. Since the key to studying these transitions is the calculation of $\Omega^s(h; \mu, T)$, this problem is ideally suited to the smoothed DFT approach taken here.^{32,33} This theory has previously been applied to

wetting and drying phenomena³⁴ and has proven to be especially accurate in predicting wall–fluid interfacial properties in the absence of collective fluctuations.³⁵

The surface grand potential, Ω^s , can be evaluated from its defining equation,³⁶

$$\Omega^s \equiv \Omega + p_b V, \quad (2)$$

where p_b is the bulk pressure and V is the total volume occupied by the fluid.

When applied to wall–fluid interfaces, the smoothed DFT theory is defined by a grand ensemble potential functional Ω of the form

$$\begin{aligned} \Omega = & F^{\text{ex}}[\bar{\rho}] + k_B T \int d\mathbf{r} \rho(\mathbf{r}) \{ \ln[\Lambda^3 \rho(\mathbf{r})] - 1 \} \\ & + \int d\mathbf{r} \rho(\mathbf{r}) [V_{\text{ext}}(\mathbf{r}) - \mu], \end{aligned} \quad (3)$$

where $\bar{\rho}$ is the coarse-grained density profile, k_B is the Boltzmann constant, $\rho(\mathbf{r})$ is the number density distribution, $\Lambda \equiv (h^2/2m\pi k_B T)^{1/2}$ denotes the translational de Broglie wavelength, and μ and T are the bulk thermodynamic fields (chemical potential and temperature, respectively). $V_{\text{ext}}(\mathbf{r})$ is a one-body external field and $F^{\text{ex}}[\rho]$ is the excess-free-energy functional and is defined in terms of a separation of the bulk equation of state into a hard-sphere term (HS) and an attractive interaction term (α) and two associated coarse-grained density profiles ($\bar{\rho}_{\text{HS}}, \bar{\rho}_\alpha$):

$$F^{\text{ex}}[\rho] = \int d\mathbf{r} \rho(\mathbf{r}) [\Delta \psi_{\text{HS}}(\bar{\rho}_{\text{HS}}(\mathbf{r})) + \Delta \psi_\alpha(\bar{\rho}_\alpha(\mathbf{r}))], \quad (4)$$

$$\bar{\rho}_i(\mathbf{r}) = \int d\mathbf{r}' \rho(\mathbf{r}') \omega_i(|\mathbf{r} - \mathbf{r}'|, \bar{\rho}_i(\mathbf{r})), \quad i \in \{\text{HS}, \alpha\}, \quad (5)$$

where the $\omega_i(|\mathbf{r} - \mathbf{r}'|, \rho)$ are density weight functions^{25,37} (usually restricted to homogeneous fluid forms) and $\Delta \psi = \Delta \psi_{\text{HS}} + \Delta \psi_\alpha$ denotes the excess free energy per particle of a homogeneous fluid (of number density ρ). The HS term is taken to be Carnahan–Starling’s result as in Ref. 25. The attractive term has tended to be treated in strict mean field:

$$\Delta \psi_\alpha(\bar{\rho}_\alpha(\mathbf{r})) = -\frac{1}{2} \alpha \bar{\rho}_\alpha(\mathbf{r}), \quad (6)$$

$$\alpha \equiv - \int d\mathbf{r} \phi_\alpha(|\mathbf{r} - \mathbf{r}'|), \quad (7)$$

$$\bar{\rho}_\alpha(\mathbf{r}) = -(1/\alpha) \int d\mathbf{r}' \rho(\mathbf{r}') \phi_\alpha(|\mathbf{r} - \mathbf{r}'|), \quad (8)$$

where $\phi_\alpha(\mathbf{r})$ denotes the attractive part of the intermolecular pair potential. Here we follow Ref. 33, and set the attractive fluid–fluid correlation term to:

$$\begin{aligned} \Delta \psi_\alpha(\rho)/k_B T = & C_1(T)\rho + C_2(T)\rho^2 + C_3(T)\rho^3 \\ & + C_4(T)\rho^4 + C_5(T)\rho^5. \end{aligned} \quad (9)$$

This expression reflects the equation of state used in our calculations, which combines a five term virial expansion in density, for the attractions, with a hard-sphere term describing repulsions:

$$\begin{aligned} \beta p_b = & \beta p_{\text{HS}}(\rho) + C_1(T)\rho^2 + 2C_2(T)\rho^3 + 3C_3(T)\rho^4 \\ & + 4C_4(T)\rho^5 + 5C_5(T)\rho^6, \end{aligned} \quad (10)$$

where $\beta = 1/k_B T$, the hard-sphere pressure p_{HS} is given by the Carnahan–Starling equation of state¹⁷ and the coefficients C_1 – C_5 were taken to be a function of temperature only, as suggested in Ref. 17.

In the model considered here, oscillations in density occur only perpendicular to the plates. This direction is designated z . A Lennard-Jones (LJ) potential, characterized by the energy ε and the particle diameter σ , was chosen for the fluid–fluid interactions. This potential is cut and shifted at a separation of $r_c = 2.5\sigma$. To obtain the attractive part of the interactions the potential is split at the position³⁸ of the potential minimum: $r_{\min} = 2^{1/6}\sigma$, thus

$$\phi_a(r) = \begin{cases} \phi_{LJ}(r_{\min}) - \phi_{LJ}(r_c), & r \leq r_{\min}, \\ \phi_{LJ}(r) - \phi_{LJ}(r_c), & r_{\min} < r \leq r_c, \\ 0, & r > r_c, \end{cases} \quad (11)$$

where the LJ potential is defined as

$$\phi_{LJ}(r) = 4\varepsilon \left[\left(\frac{\sigma}{r} \right)^{12} - \left(\frac{\sigma}{r} \right)^6 \right]. \quad (12)$$

The wall–fluid potential is defined as a cut and shifted 9–3 LJ potential:

$$V_{\text{ext}}(z) = \begin{cases} \phi_{9-3}(z) - \phi_{9-3}(z_c), & z \leq z_c, \\ 0, & z > z_c, \end{cases} \quad (13)$$

where

$$\phi_{9-3}(z) = \sqrt{\frac{2}{5}} \varepsilon_{\text{wf}} \left[\frac{1}{5} \left(\frac{\sigma_{\text{wf}}}{z} \right)^9 - \frac{3}{2} \left(\frac{\sigma_{\text{wf}}}{z} \right)^3 \right], \quad (14)$$

$z_c = 2.5\sigma$, $\sigma_{\text{wf}} = \sigma$, and ε_{wf} is the potential well depth which we vary to control the wetting properties of the fluid on the wall.

In order to isolate the effects of the solvation forces, the wall–wall potential is initially set to zero:

$$V_{\text{ww}}(z) = \begin{cases} \infty, & z < 0 \\ 0, & z \geq 0. \end{cases} \quad (15)$$

When we do include a nonzero interaction potential between the two surfaces, we consider the walls to be thin plates (i.e., one molecule thick) interacting via a 9–3 LJ potential represented by Eqs. (16) and (17)

$$V_{\text{ww}}(z) = \begin{cases} \phi_{9-3}(z) - \phi_{9-3}(z_c), & z \leq z_c \\ 0, & z > z_c \end{cases}, \quad (16)$$

$$\phi_{9-3}(z) = \sqrt{\frac{2}{5}} \varepsilon_{\text{ww}}^* \left[\frac{1}{5} \left(\frac{\sigma_{\text{ww}}}{z} \right)^9 - \frac{3}{2} \left(\frac{\sigma_{\text{ww}}}{z} \right)^3 \right]. \quad (17)$$

The diameter of the wall particles is set equal to that of the fluid, $\sigma_{\text{ww}} = \sigma$, and $\varepsilon_{\text{ww}}^* = \varepsilon_{\text{ww}}/\varepsilon$, is the reduced well depth which determines the strength of the particle interactions that make up the plate. The value of the z_c/σ is $(2/5)^{1/6}$ when we want to consider purely repulsive wall–wall interactions, and is set to 2.5 when both repulsive and attractive interactions are included.

The degree of wetting may be characterized by the cosine of the contact angle θ , which ranges from -1 to 1 . The

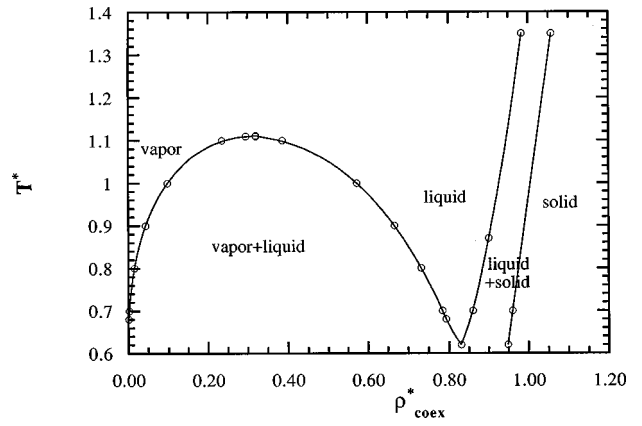


FIG. 1. The coexistence density ($\rho_{\text{coex}}^* = \rho_{\text{coex}}\sigma^3$)–temperature ($T^* = k_B T/\varepsilon$) phase diagram for the LJ fluid. The triple point temperature is 0.62 and the critical point is 1.11.

contact angle describes the equilibrium thermodynamics of adsorbed fluids at bulk two-phase coexistence and is defined by the equation:³⁵

$$\Omega_{LV}^s \cos \theta = \Omega_{WV}^s - \Omega_{WL}^s. \quad (18)$$

In a macroscopic system, Eq. (18) is often considered a force balance between coexisting liquid (L) and vapor (V) in the presence of a wall (W). Clearly, in order to model a contact angle measurement properly, one needs to be able to obtain wall–liquid (WL) and wall–vapor (WV) surface free energies at specified values of the bulk fluid boundary conditions. Because of our desire to link surface free energies and solvation forces, we chose to work with the smoothed DFT, since it can accurately calculate surface free energies at an interface.

When $\cos \theta = -1$, complete drying conditions hold, the wall is in contact with a gaseous film, and is described as dry. When $-1 < \cos \theta < 1$, the surface is partially wet by the fluid, while at $\cos \theta = 1$ the wall is wet by a macroscopic film of liquid and is considered a completely wetting phase.³⁵

A. Partial wetting: $-1 < \cos \theta < 1$

In this section we concentrate on the partial wetting state and distinguish two cases. If the colloid surface likes the solvent, $\cos \theta > 0$, we call this a *solvophilic surface*, whereas if the surface dislikes the solvent, $\cos \theta < 0$, we refer to it as a *solvophobic surface*. We will consider how the solvation potential per unit area, Ω^s/A , changes with the $\cos \theta$, the temperature, and the bulk density of the system. Direct wall–wall interactions are taken to be hard [Eq. (15)]. Figure 1 gives the density–temperature coexistence envelope for the LJ fluid as calculated by the equation of state described in Eq. (10).

Figure 2 shows the reduced surface grand potential $\Omega^{s*}/A = \Omega^s \sigma^2/(A\varepsilon)$ for a solvophilic surface as a function of the separation distance between the two walls, scaled by the solvent diameter σ . The solvation potential is shown for two different values of the reduced bulk density, $\rho_b^* = \rho_b \sigma^3$. An interesting phenomenon takes place at a bulk density $\rho_b^* = 0.01$, which is a vapor density. At a separation of $h/\sigma \approx 5.7$, a break in the slope of the potential occurs. This

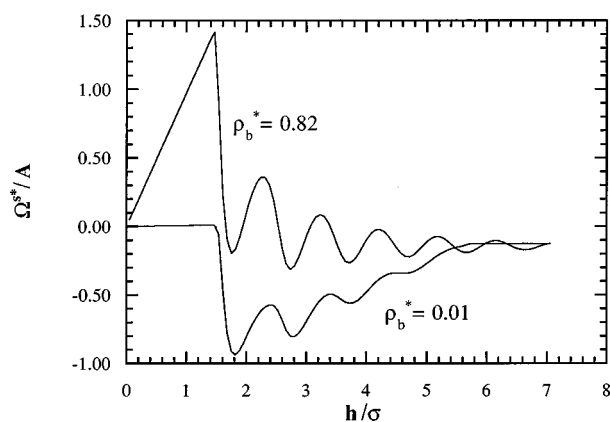


FIG. 2. Solvation potentials per unit area for a solvophilic surface. $\epsilon_w^* = 2.8$, $\cos \theta = 0.8328$ and $T^* = 0.8$.

is an indication that *capillary condensation* has occurred. Capillary condensation is a first-order phase transition where the confined fluid changes from a vaporlike state into a liquidlike state while the bulk is still a vapor. Here the transition occurs when surface separation of the two parallel plates is decreased. The reverse of this phenomenon, *capillary evaporation*, occurs when the confined fluid turns into a vaporlike state when the bulk fluid is still a liquid.¹⁷ Capillary evaporation is expected when the surfaces are solvophobic. To further demonstrate that capillary condensation has occurred, we plot in Fig. 3 the density profiles at $h/\sigma = 5.5$, and $h/\sigma = 6$ for $\rho_b^* = 0.01$. A vaporlike density profile is found at $h/\sigma = 6$, while a liquidlike profile is present at $h/\sigma = 5.5$. Figure 4 shows the solvation potentials for a solvophobic surface at two different bulk densities. Comparing with Fig. 2, we note that the amplitude of the solvation potential is reduced upon decreasing $\cos \theta$. For $\rho_b^* = 0.01$, the energy barrier between the solvation minima gradually disappears as the surface becomes more solvophobic.

B. Phase transitions of colloidal systems

The primary topics of this paper are transitions in plate spacing and the determination of phase diagrams for colloidal surfaces with different wetting properties. As mentioned,

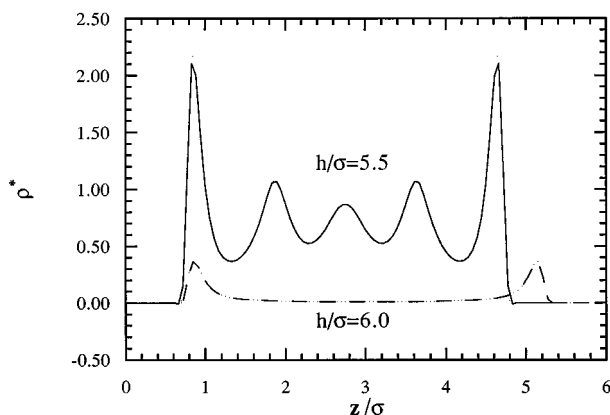


FIG. 3. Density profiles for wall separations of $h/\sigma = 5.5$ and $h/\sigma = 6.0$ for $\rho_b^* = 0.01$, $T^* = 0.8$, $\epsilon_w^* = 2.8$, $\cos \theta = 0.8328$. The $h/\sigma = 5.5$ case exhibits a liquidlike profile while the $h/\sigma = 6.0$ shows a vaporlike profile.

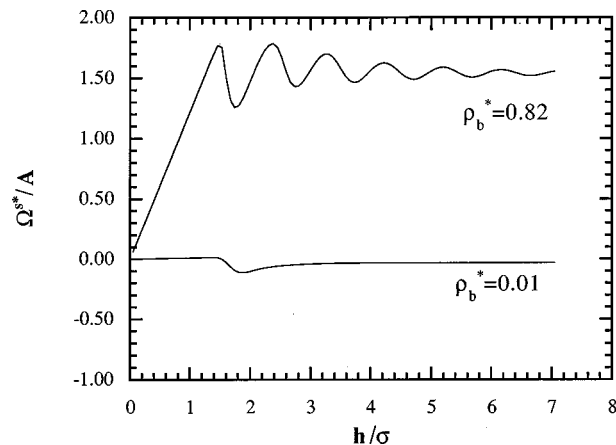


FIG. 4. Solvation potentials per unit area for a solvophobic surface. $\epsilon_w^* = 1.68$, $\cos \theta = -0.1176$, and $T^* = 0.8$.

the key to studying these transitions is the calculation of the surface grand potential. The global minimum in the surface grand potential defines the stable equilibrium phase. As the surface field and the bulk conditions are varied, the location of the global minimum may change abruptly, signaling a discontinuous phase transition in plate separation.

Figure 5 shows an oscillatory surface potential with three energy minima. The first minimum occurs at an equilibrium separation of 0.05 solvent diameters and corresponds to a collapsed phase, i.e., the two plates are in contact, excluding the solvent completely. The second minimum occurs at a separation of two molecular diameters. For this case there is only a single layer of solvent between the surfaces. Adopting the terminology used for clays,⁸ we refer to this state as the crystalline state. This does not imply that the confined fluid is anything other than fluid, rather it refers to the fact that in clay systems a stack of clay platelets would have the appearance of a crystal. Finally, there is the so-called swollen phase, with two layers of confined fluid characterized by the third minimum which is found around a separation of three solvent diameters. Figure 6 displays the density profiles for both the crystalline and swollen phases.

To determine the equilibrium state of the system and generate phase diagrams we proceeded as follows. We fix the

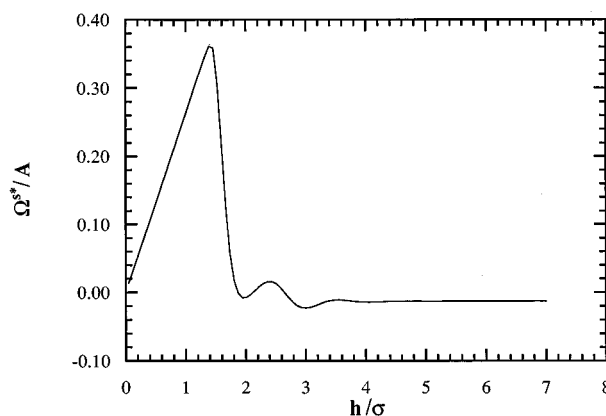


FIG. 5. Solvation potential per unit area for $T^* = 1.4$, $\rho_b^* = 0.3$, $\epsilon_w^* = 1.71$, $\cos \theta = 0.0017$.

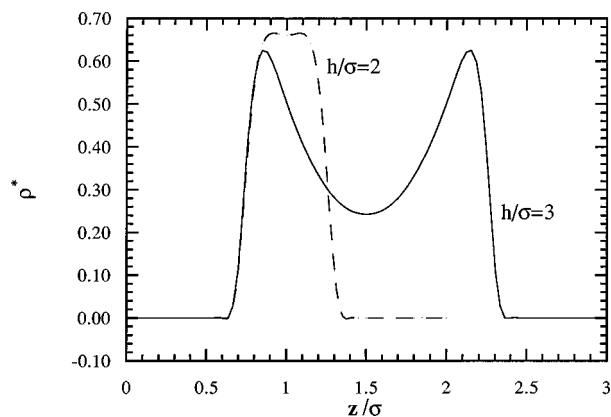


FIG. 6. Density profiles for $T^*=1.4$, $\rho_b^*=0.3$, $\epsilon_w^*=1.71$, and $\cos \theta=0.0017$, at surface separations of 2σ (crystalline phase) and 3σ (swollen phase).

temperature, T , the strength of the wall–fluid interaction potential, ϵ_w , the bulk density, ρ_b , and we calculate the solvation potential per unit area, Ω^s/A , for a plate separation ranging from $h=0.05\sigma$ to 7σ , using a step size of 0.05σ . We continue by increasing the bulk density for this temperature. A complete phase diagram can then be constructed by repeating the procedure for the temperatures of interest. The temperature range considered here is $0.66 < Tk_B/\epsilon < 2$, which corresponds to the range of applicability of the equation of state used in the DFT.³⁹ For methanol, for example, $\epsilon=6.383 \times 10^{-21}$ J,⁴⁰ and therefore this range corresponds to $32^\circ\text{C} < T < 651.5^\circ\text{C}$ and for cyclohexane, $\epsilon=6.893 \times 10^{-21}$ J⁴⁰ and $56.3^\circ\text{C} < T < 725.4^\circ\text{C}$.

III. RESULTS

A. Phase diagrams

In this section we will explore the effects of the solvation forces on the equilibrium separation of parallel plates. To highlight the role of solvation forces we set the direct wall–wall interactions to zero [Eq. (15)] and restrict ourselves to solvent–solvent and solvent–wall interactions. This constraint is relaxed in the next sections.

Figure 7 shows the bulk density–temperature phase diagrams for (a) a solvophilic surface, $\cos \theta=0.9277$ and $\theta \approx 22^\circ$, (b) a “neutral” surface, whose $\cos \theta=0.0014$ and $\theta \approx 90^\circ$, and (c) a solvophobic surface, $\cos \theta=-0.2657$ and $\theta=105.4^\circ$. Three phases are observed as defined in the previous section: the swollen, the crystalline, and the collapsed phase. In Fig. 7(a) the collapsed phase occupies a relatively small portion of the diagram. This is to be expected; since the surfaces like the solvent, it is reasonable to find some fluid between the two walls. However, increasing the temperature stabilizes the collapsed state. We note that the collapsed state is the only state observed for a system of hard spheres between hard walls, and this is most likely a property of purely repulsive fluids between purely repulsive walls. Since our system in the high temperature limit approaches such a purely repulsive system, we would expect the collapsed phase to prevail at high temperatures. The crystalline phase is more common than the swollen phase. The swollen

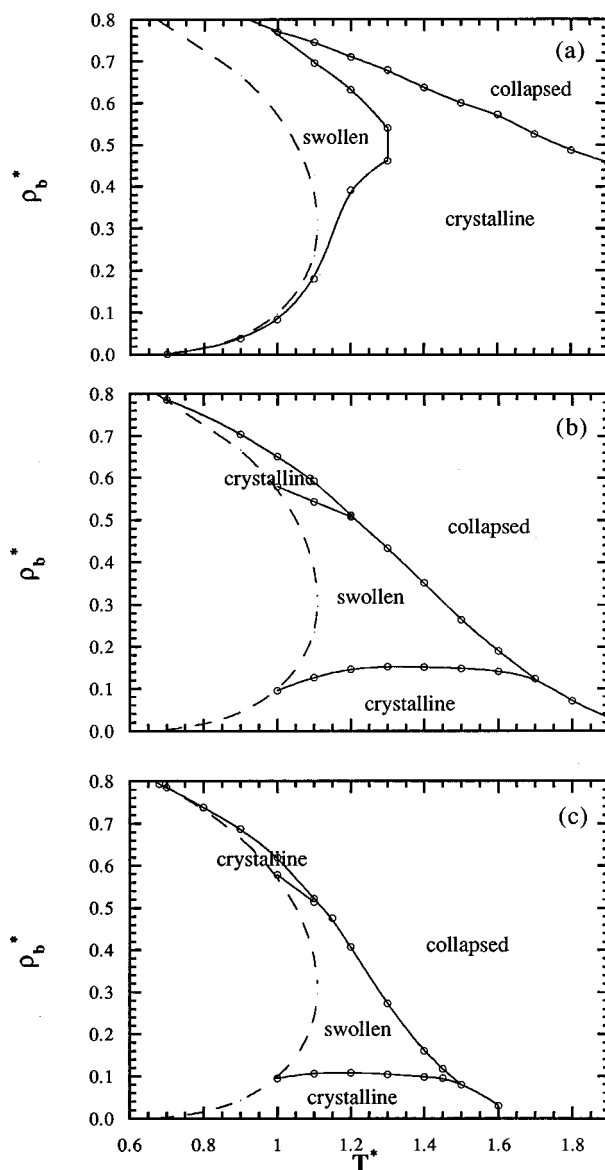


FIG. 7. Bulk density–temperature phase diagrams. The dotted line is the liquid–vapor coexistence bulk density. (a) Phase diagram for a solvophilic surface. $\epsilon_w^*=2.8$, $\cos \theta=0.9277$. (b) Phase diagram for a “neutral” surface, $\epsilon_w^*=1.71$, $\cos \theta=0.0014$. (c) Phase diagram for a solvophobic surface. $\epsilon_w^*=1.44$, $\cos \theta=-0.2657$.

phase is present at lower temperature, $T^*=k_B T/\epsilon \leq 1.3$. For a fixed bulk density the general trend is to see decreased swelling with increasing temperature.

Figure 7(b) presents the phase diagram for a “neutral” surface. The surface can be considered either solvophilic or solvophobic, since the contact angle is virtually 90° . The phase diagram is quite different from the one in Fig. 7(a). The collapsed phase dominates more, and generally speaking the phase transitions have shifted to lower bulk densities. We no longer exclusively observe at most bulk densities the simple trend of a stepwise decreased swelling with increased temperature. Instead, we also find transitions between a swollen and a collapsed state. The swollen state is only present for an intermediate range of temperatures and densities.

Figure 7(c) presents the density–temperature diagram for a solvophobic surface. The phase diagram is qualitatively similar to the phase diagram for the “neutral” surface. The collapsed state is even more predominant, and the regions where one observes the other states have more or less shrunk uniformly.

B. The role of repulsive wall–wall interactions

This and the next section focus on the role of direct interactions between two surfaces. In this section we will only consider purely repulsive wall–wall interactions. The functional form of the latter is given by Eqs. (16) and (17) with $z_c/\sigma = (2/5)^{1/6} = 0.8584$.

The phase transitions are rather insensitive to the strength of the wall–wall interaction. This stems from the short range of the potential. We generated results for a solvophilic surface, $\epsilon_w^* = 2.8$, where $\epsilon_w^* = \epsilon_{wf}/\epsilon$, $\cos \theta = 0.9277$, for two values of the $\epsilon_{ww}^* = 1.5$ and 1, and have found identical phase diagrams. Hence, we will restrict the discussion to a single value of the wall–wall strength, namely $\epsilon_{ww}^* = 1$. Figure 8(a) presents the bulk density–temperature phase diagram. The diagram clearly illustrates that for a solvophilic surface the collapsed phase is suppressed over this range of temperatures. With the wall–wall repulsion present, plates in direct contact experience a large positive energy. In other words, with a wall–wall repulsion acting, two plates have a nonzero excluded volume. When the surfaces are immersed into a fluid, the collapsed state is considerably less favorable compared to the zero wall–wall interaction.

For low temperatures, up to $T^* = 1.3$, the following set of transitions is observed, as the bulk density is increased: starting from a crystalline phase one enters the swollen state and then returns to the crystalline phase. The crystalline phase is most prevalent and is the only relevant phase at high temperatures.

Figure 8(b) shows the bulk density–temperature phase diagram for a “neutral” surface, $\epsilon_w^* = 1.71$, $\cos \theta = 0.0014$ and $\epsilon_{ww}^* = 1$. Reducing the wall–fluid interactions brings back the collapsed phase into the phase diagram, but compared to the zero wall–wall interaction shown in Fig. 7(b), the collapsed phase is much less dominant. For high densities, the walls are in contact, and as the density is decreased there are either one or two layers of fluid at all temperatures considered.

The phase diagram for a solvophobic surface is presented in Fig. 8(c). This plot appears very similar to the previous one. The main difference is that the transition from the crystalline to a collapsed phase has been shifted to lower densities, making the collapsed phase more common. From this and from a comparison of Figs. 7(b) and 7(c), we conclude that the phase diagrams for a “neutral” and solvophobic surface are qualitatively the same.

C. Effect of repulsive and attractive wall–wall interaction

In this section we extend the wall–wall interactions to include both repulsive and attractive contributions. A repre-

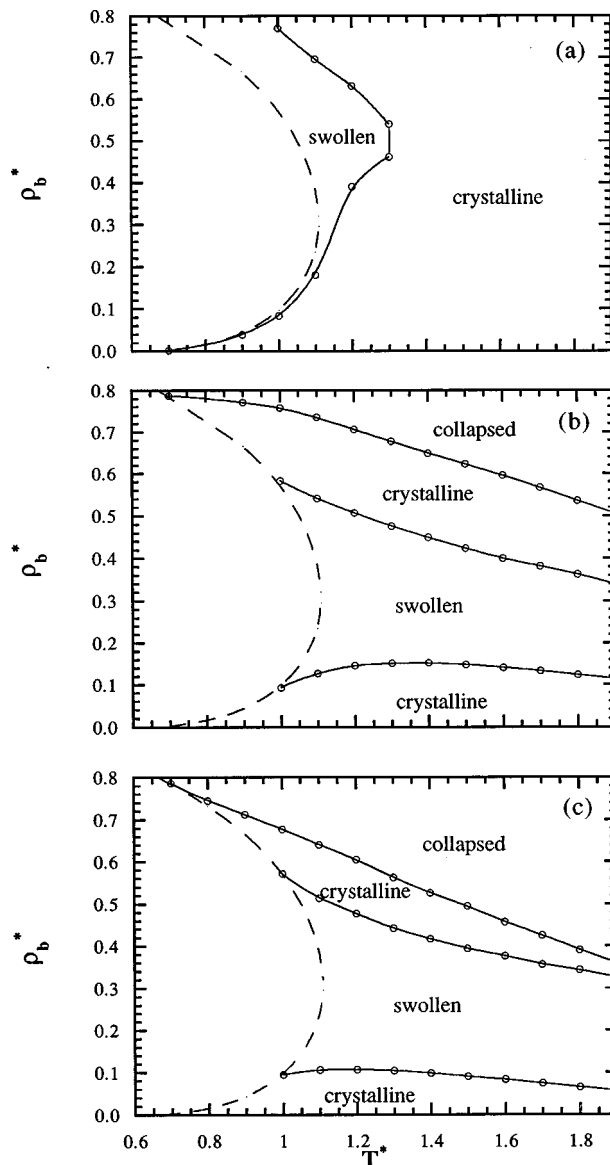


FIG. 8. Bulk density–temperature phase diagrams. The dotted line is the liquid–vapor coexistence bulk density. (a) Surfaces are solvophilic. $\epsilon_w^* = 2.8$, $\cos \theta = 0.9277$, $\epsilon_{ww}^* = 1$, and $z_c = 0.86\sigma$. (b) $\epsilon_w^* = 1.71$, $\cos \theta = 0.0014$ (“neutral” surface), $\epsilon_{ww}^* = 1$, and $z_c = 0.86\sigma$. (c) $\epsilon_w^* = 1.44$, $\cos \theta = -0.2657$ (solvophobic surface), $\epsilon_{ww}^* = 1$, and $z_c = 0.86\sigma$.

sentative potential is the 9–3 LJ potential, cut and shifted at $z_c = 2.5\sigma$. This potential is defined by Eqs. (16) and (17).

In contrast to the purely repulsive case, the strength of the wall–wall interactions does play an important role. We start with the bulk density–temperature phase diagram for a solvophilic surface [Fig. 9(a)], where $\epsilon_w^* = 2.8$, $\cos \theta = 0.9277$ and $\epsilon_{ww}^* = 1$. For low temperatures and low densities the walls are in contact. By increasing the density, the system goes to the crystalline and finally to the swollen state. This transition is illustrated in more detail in Fig. 9(b), for temperatures up to $T^* = 0.8$, and densities up to $\rho_b^* = 0.01$. The swollen phase occupies only a small part of the phase diagram. The phase boundaries of the three phases approach each other very closely around $\rho_b^* = 0.002$ and $T^* = 0.71$. We have not resolved these boundaries in enough detail to decide whether there exists triple points in this region.

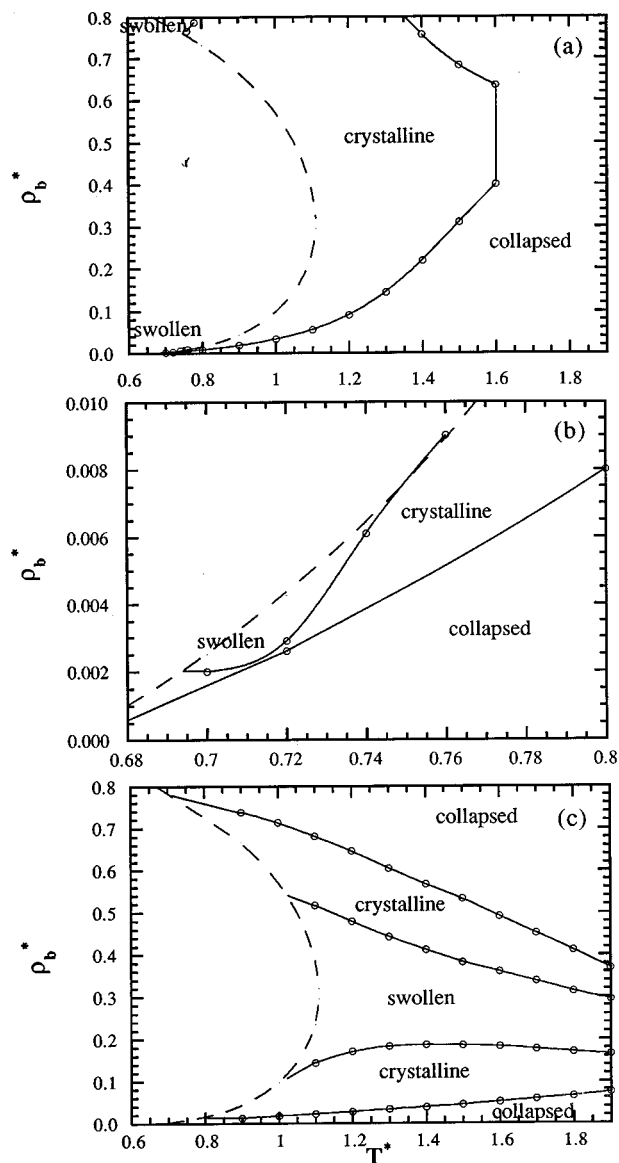


FIG. 9. Bulk density-temperature phase diagrams. The dotted line is the liquid-vapor coexistence bulk density. (a) Phase diagram for a solvophilic surface. $\epsilon_w^* = 2.8$, $\cos \theta = 0.9277$, $\epsilon_{ww}^* = 1$, and $z_c = 2.5\sigma$. (b) Details from the bulk density-temperature phase diagram in Fig. 9(a), for small temperatures and densities. (c) Surfaces are "neutral." $\epsilon_w^* = 1.71$, $\cos \theta = 0.0014$, $\epsilon_{ww}^* = 0.1$, and $z_c = 2.5\sigma$.

Above $T^* = 0.8$ we no longer observe the swollen state, and the only transitions are those between a collapsed and a crystalline phase. Finally, for high temperatures, $T^* > 1.6$, only the collapsed state is found.

When the colloidal surfaces are "neutral" or solvophobic, the collapsed phase extends over the entire phase diagram. This is true for both $\epsilon_{ww}^* = 1$ and 0.5. In order to stabilize other phases for the "neutral" surface, the strength of the attractive wall-wall potential must be significantly reduced. At a value of $\epsilon_{ww}^* = 0.1$, the density-temperature phase diagram does display all phases [see Fig. 9(c)]. At low temperatures the stable phase is the collapsed state. At higher temperatures the phase diagram is more similar to that found for the purely repulsive wall-wall interaction [cf Fig. 8(b) 8(c)]. However, the wall-wall attractions introduce the col-

lapsed phase at low densities, where the fluid is unable to push the plates apart. This applies to all types of wall-fluid interactions.

IV. CONCLUSIONS AND DISCUSSION

The simple colloidal model of parallel plates (or walls) investigated here exhibits three possible phases: swollen, crystalline, and collapsed. As the solvent conditions vary, i.e., when the bulk density or temperature are changed, transitions between these states of plate separation occur. The wetting properties of the single plate fluid interface play a key role in shaping the phase diagrams. We have chosen to characterize the solvent/surface interactions through the contact angle at $T^* = 0.8$ to facilitate experimental identification. In the partial wetting regime the contact angle is, of course, a sensitive function of the strength of the wall-fluid potential.

When the surface is solvophilic and no direct wall-wall interactions exist, the most dominant phase occurs when the plates are separated by a single solvent layer. For solvophobic surfaces the most frequently encountered state is the collapsed state that entirely excludes confined fluid. The phase diagrams for a "neutral" and a solvophobic surface are very similar, suggesting that the phase diagram is relatively insensitive to the wall-fluid strength once the contact angle is larger than 90 deg.

When the repulsive part of the wall-wall interaction is taken into account, the collapsed phase is suppressed. Due to the short range of the repulsive potential considered, the phase diagrams are insensitive to the strength of a purely repulsive wall-wall interaction.

The phase diagrams are much more sensitive to the strength of the surface/surface potential when attractions are included. It appears that for a "neutral" and solvophobic surface, only one (collapsed) phase is observed, independent of the bulk density or temperature. Only for very small values of the wall-wall strength do we see phase transitions. Finally, we note that in the presence of wall-wall attractions, the phase diagrams always exhibit a collapsed phase at low bulk densities, as opposed to the crystalline phase.

Experimental systems that also have the simple parallel plate geometry considered here, and which display phase transitions driven by solvation forces, include clay suspensions. Clays such as smectite,¹⁰ sodium montmorillonite,^{42,43} lithium and potassium montmorillonite and lithium vermiculite,⁴³ all exhibit a swollen phase that is a twofold expansion of the crystalline phase, while *n*-butylammonium vermiculite^{8,9} shows a sixfold expansion. Certain clays, such as potassium and cesium vermiculite and cesium montmorillonite, are collapsed in dilute electrolyte solutions,⁴³ whereas clays like mica,^{11,43,44} kaolinite, and illite¹⁰ do not swell at all.

As we have demonstrated, our model system exhibits a swollen phase that is a twofold expansion of the crystalline, and further, under different conditions, the system can be found in a collapsed state. This quantitative difference, i.e., no sixfold expansions, in swelling behavior was expected for several reasons. Our colloidal model is highly simplified, the plates are both perfectly smooth and rigid, and we have not included the effects of ions and surface charges. Also, the

results that have been presented here are for the case of $r_c = z_c = 2.5\sigma$, for the fluid–fluid and wall–fluid interactions, respectively. With longer cutoffs,¹⁷ the first two minima are shallower than those at larger separations, suggesting that the equilibrium configuration for the colloidal system may occur at larger separations. However, we would not expect the qualitative results to change from the case of $r_c = z_c = 2.5\sigma$. We believe that the present model captures important aspects of the physics, particularly the dependence on the bulk conditions and the role of the direct wall–wall interactions. Moreover, it is relatively straightforward to extend the current approach of determining equilibrium separations to a system containing charged ions and neutral solvent as was recently shown by Frink and van Swol.⁴⁵

Clays that do not swell spontaneously, like mica for example, appear to have a high surface charge density. This high lattice charge apparently prevents swelling and in fact a large amount of work is required in order to initially separate the crystal along the basal plane in water.¹¹ It has also been shown that once the mica crystal has been forced apart and the surfaces exposed to electrolyte solution they no longer readhere.⁴⁶ The surfaces then behave like a swelling clay, and it is for this system that it is feasible to accurately measure the force interaction from large separations down to about the last molecular layer of water.¹¹ This nonswelling behavior cannot be predicted with our model because of its lack of charges.

In conclusion, the phase diagrams presented in this paper give a qualitative idea of swelling transitions in a colloidal system. In particular, we have illustrated the role of the bulk state point and the degree of surface/surface and solvent/surface affinity. The approach presented here can be extended to include ions and surface charges (see Ref. 45). In essence, such an extension would constitute an augmented DLVO theory of colloid stability. It would capture the familiar dependence on surface charge and added salt of traditional DLVO theory, as well as the role of hydrostatic pressure and wetting properties presented here.

ACKNOWLEDGMENTS

The authors thank C. F. Zukoski for many helpful discussions. This work was supported by NASA under Grant No. NAG8-976.

¹B. V. Derjaguin and L. Landau, *Acta Physicochim. URSS* **14**, 633 (1941).

²E. J. W. Verwey and J. Th. G. Overbeek, *Theory of Stability of Lyophobic Colloids* (Elsevier, Amsterdam, 1948).

³J. N. Israelachvili, *Intermolecular and Surface Forces*, 2nd ed. (Academic, San Diego, 1992).

- ⁴R. P. Rand and V. A. Parsegian, *Biochim. Biophys. Acta* **988**, 351 (1989).
- ⁵D. C. Rau and V. A. Parsegian, *Biophys. J.* **61**, 246 (1992).
- ⁶S. Leikin, D. C. Rau, and V. A. Parsegian, *Biophys. J.* **64**, A270 (1993).
- ⁷D. C. Rau and V. A. Parsegian, *Science* **249**, 1278 (1990).
- ⁸L. F. Braganza, R. J. Crawford, M. V. Smalley, and R. K. Thomas, *Clays Clay Miner.* **38**, 90 (1990).
- ⁹M. V. Smalley, R. K. Thomas, L. F. Braganza, and T. Matsuo, *Clays Clay Miner.* **37**, 474 (1989).
- ¹⁰K. K. Mohan, R. N. Vaidya, M. G. Reed, and H. Scott Fogler, *Colloids Surf.* **73**, 237 (1993).
- ¹¹R. M. Pashley and J. P. Quirk, *Colloids Surf.* **9**, 1 (1984).
- ¹²Y. Horikawa, R. S. Murray, and J. P. Quirk, *Colloids Surf.* **32**, 181 (1988).
- ¹³D. C. Rau and V. A. Parsegian, *Biophys. J.* **61**, 260 (1992).
- ¹⁴S. Leikin, D. C. Rau, and V. A. Parsegian, *Phys. Rev. A* **44**, 5272 (1991).
- ¹⁵E. Ya. Rode and N. A. Krotov, *J. Inorg. Chem. USSR* **4**, 804 (1959).
- ¹⁶V. I. Spitsyn and I. D. Kolli, *J. Inorg. Chem. USSR* **1**, 2403 (1956).
- ¹⁷L. J. D. Frink and F. van Swol, *J. Chem. Phys.* **100**, 9106 (1994).
- ¹⁸R. G. Horn and J. N. Israelachvili, *J. Chem. Phys.* **75**, 1400 (1981).
- ¹⁹S. J. O'Shea, M. E. Welland, and T. Rayment, *Appl. Phys. Lett.* **60**, 2356 (1992).
- ²⁰J. J. Magda, M. Tirrell, and H. T. Davis, *J. Chem. Phys.* **86**, 1888 (1985).
- ²¹J. N. Israelachvili and P. M. McGuiggan, *Science* **241**, 795 (1988).
- ²²S. G. Ash, D. H. Everett, and C. Radke, *J. Chem. Soc. Faraday Trans. 2* **69**, 1256 (1973).
- ²³R. Evans and U. Marini Bettolo Marconi, *J. Chem. Phys.* **86**, 7138 (1987).
- ²⁴M. Lupkowski and F. van Swol, *J. Chem. Phys.* **95**, 1995 (1991).
- ²⁵P. Tarazona, *Phys. Rev. A* **31**, 2672 (1985).
- ²⁶L. J. Douglas, M. Lupkowski, T. L. Dodd, and F. van Swol, *Langmuir* **9**, 1445 (1993).
- ²⁷L. H. Dubois, B. R. Zegarski, and R. G. Nuzzo, *J. Am. Chem. Soc.* **112**, 570 (1990).
- ²⁸H. A. Biebuyck, C. D. Bain, and G. M. Whitesides, *Langmuir* **10**, 1825 (1994).
- ²⁹P. E. Laibinis, R. G. Nuzzo, and G. M. Whitesides, *J. Phys. Chem.* **96**, 5097 (1992).
- ³⁰C. D. Bain and G. M. Whitesides, *J. Am. Chem. Soc.* **110**, 3665 (1988).
- ³¹Ya. I. Rabinovich and R.-H. Yoon, *Langmuir* **10**, 1903 (1994).
- ³²F. van Swol and J. R. Henderson, *Phys. Rev. A* **40**, 2567 (1989).
- ³³F. van Swol and J. R. Henderson, *Phys. Rev. A* **43**, 2932 (1991).
- ³⁴J. R. Henderson, P. Tarazona, F. van Swol, and E. Velasco, *J. Chem. Phys.* **96**, 4633 (1992).
- ³⁵P. Adams and J. R. Henderson, *Mol. Phys.* **73**, 1383 (1991).
- ³⁶J. R. Henderson and F. van Swol, *Mol. Phys.* **56**, 1313 (1985).
- ³⁷P. Tarazona, U. Marini Bettolo Marconi, and R. Evans, *Mol. Phys.* **60**, 573 (1987).
- ³⁸J. D. Weeks, D. Chandler, and H. C. Andersen, *J. Chem. Phys.* **54**, 5237 (1971).
- ³⁹Note that the triple point and critical temperatures of the cut and shifted LJ fluid are $k_B T_t / \epsilon = 0.62$ and $k_B T_c / \epsilon = 1.11$, respectively.
- ⁴⁰The critical temperature of the cut and shifted LJ fluid is $k_B T_c / \epsilon = 1.11$. The critical temperature of methanol is 513.15 K (Ref. 41), so $\epsilon = 6.383 \times 10^{-21}$ J for the methanol–methanol interaction. For cyclohexane, $T_c = 554.15$ K (Ref. 41), so $\epsilon = 6.893 \times 10^{-21}$ J.
- ⁴¹R. H. Perry and D. Green, *Perry's Chemical Engineers' Handbook*, 6th ed. (McGraw-Hill, 1984).
- ⁴²K. Norrish and J. P. Quirk, *Nature (London)* **173**, 255 (1954).
- ⁴³J. P. Quirk, *Isr. J. Chem.* **6**, 213 (1968).
- ⁴⁴A. Delville, *J. Phys. Chem.* **97**, 9703 (1993).
- ⁴⁵L. J. D. Frink and F. van Swol, *J. Chem. Phys.* (in press).
- ⁴⁶R. M. Pashley, *J. Colloid Interface Sci.* **83**, 531 (1981).